Journal of Power Sources 192 (2009) 51–56

Contents lists available at ScienceDirect

Journal of Power Sources

journal homepage: www.elsevier.com/locate/jpowsour

Carbon nanofibers as electrocatalyst support for fuel cells: Effect of hydrogen on their properties in CH_4 decomposition☆

D. Sebastián, I. Suelves, M.J. Lázaro*, R. Moliner

Instituto de Carboquímica (CSIC), Miguel Luesma Castán 4, 50018 Zaragoza, Spain

ARTICLE INFO

Article history:
Received 2 October 2008
Received in revised form
24 November 2008
Accepted 25 November 2008
Available online 3 December 2008

Keywords:
Carbon nanofiber
Electrical conductivity
Electrocatalyst
PEM fuel cell
Hydrogen

ABSTRACT

The influence of low partial pressure of hydrogen on carbon nanofibers (CNFs) properties has been studied in the synthesis by methane catalytic decomposition, with the purpose of using them in polymer electrolyte fuel cells as electrocatalyst support. Using CNFs in this kind of application presents a good perspective to improve the fuel cell overall performance. CNF growth in the catalytic decomposition of methane and the characteristics which are typically required in a carbonaceous support, are influenced by hydrogen concentration, which has been studied at different temperatures. The textural, morphological and structural characteristics of the obtained CNFs have been determined by nitrogen physisorption, X-ray diffraction, electron microscopy and thermogravimetry. Electrical conductivity of CNFs has been measured compressing the powder and using a two-probe method. It was observed that low values of partial pressure of hydrogen in methane influence positively structural ordering of CNFs, and in turn improve electrical conductivity, with a slight influence on textural properties leading to highly mesoporous carbon.

1. Introduction

Fuel cell systems are attracting more and more attention in recent years as important energy converting devices in a medium-long term future. Among the several existing types, polymer electrolyte fuel cells (PEMFC and DMFC) have favorable advantages in transport, portable and micropower applications in terms of high efficiency, high energy density, quick start-up and zero or low emission.

Although great progress has been made in the last years, the commercialization of this technology has several technical and economical barriers that must be addressed in terms of cost, durability and performance. The reduction of the required platinum loading has always been the main focus of PEMFC electrode research and development, both for reasons of cost and availability. Current electrodes have Pt loadings in the order of 0.4 mg cm^{-2}. The challenge remains in decreasing Pt loading up to 0.15 mg cm^{-2} or less, while maintaining or even increasing the performance and durability [1,2].

Currently, carbon black supports (Vulcan XC-72R, Black Pearls 2000, etc.) are widely used as platinum support, but recent publications indicate the possibility to improve the efficiency, reducing the Pt loading of the electrocatalysts, by using novel carbon supports, such as ordered mesoporous carbons [3–5], carbon aero- and xerogels [6–9], carbon nanofibers (CNFs) [10–13] and carbon nanotubes (CNTs) [13,14].

Carbon nanofilaments (CNFs and CNTs) have an excellent combination of chemical and physical properties due to their unique structure, and blend two properties that rarely coexist in a material: high surface area and high electrical conductivity [13,15,16]. Other advantage is that the catalytic nanoparticles on the external walls are easier to interact with the gases than those in the internal pores of a carbon black [17]. In both materials (CNFs and CNTs) graphite sheets form filaments with an external diameter between a few nanometers and about one hundred nanometers, but they differ in the manner by which those sheets are arranged. In a CNT, a cylinder is formed by a single sheet of graphite (single wall or SWNT) or by several concentric sheets with an increasing diameter (multi-wall or MWNT). However, CNFs are formed by graphite sheets forming a determined angle with respect to the growth axis. The main difference consists in the lack of a hollow cavity in CNFs [18].

Unlike in CNTs, the surface of CNFs is mainly present as graphite edges which are thought to give a strong interaction between the support and the active phase [19]. Additionally, the low cost and high yield of CNF production compared with CNT production would allow industry to produce high quantities of CNFs at reasonable prices [20].

The production of carbon nanofibers can be performed by decomposition of a carbon-containing gas (CH_4, C_2H_4, CO, etc.) over catalysts traditionally composed by metals of the iron subgroup (Fe, Co or Ni e.g.) and their alloys, at temperatures ranging from 400 °C to 1000 °C [15,21]. Several studies concern the relationship

☆ Presented at CONAPPICE 2008, Zaragoza, Spain, 24–26 September 2008.

* Corresponding author. Tel.: +34 976 733977; fax: +34 976 733318.
E-mail address: mlazaro@icb.csic.es (M.J. Lázaro).

0378-7753/$ – see front matter © 2008 Elsevier B.V. All rights reserved.
doi:10.1016/j.jpowsour.2008.11.092

between carbon nanofibers properties and the process by which they have been produced [19,22–25], suggesting that the final properties of the carbonaceous material depend mainly on the catalyst, carbon source and process conditions such as temperature or gas composition.

Hydrogen has several roles in carbon deposition, either accelerating or suppressing the formation of carbon, depending mainly on temperature and the carbon source used. Low concentrations of H_2 inhibit the deactivation of the catalyst by preventing the formation of encapsulating coke and helping the formation of filamentous carbon. However, increasing concentrations of H_2 lead to both a competition between H_2 and CH_4 for the catalytic active sites and the partial gasification of deposited carbon, which results in a lower yield of deposition [26,27].

In this work the aim is to study the effect of hydrogen concentration at different temperatures in the decomposition of methane on a nickel-based unsupported catalyst. The interaction of H_2 with CH_4 or with the active sites has an effect both on the yield of carbon deposition and the nature of the deposited carbon. Low reaction rates are expected to lead to a more ordered deposited carbon with larger crystal domain sizes [28], and consequently hydrogen can help to improve CNF structure and properties derived, like electrical conductivity. Morphology can also be influenced by the presence of hydrogen [24], and consequently porosity could be also affected [19]. All these mentioned characteristics presumably influence the fuel cell overall performance and have been studied in this work.

2. Experimental

2.1. Carbon nanofiber growth

Catalyst composed by $NiCuAl_2O_3$ (Ni:Cu:Al molar ratio of 78:6:16) was prepared by coprecipitation of metal nitrates, calcination at 450 °C for 8 h and reduction of 300 mg of the catalyst precursor (a mixture of the metal oxides) under a hydrogen flow of 20 mL(STP) min^{-1} at 550 °C for 3 h, as described elsewhere [29].

CNF growth was then performed in a fixed-bed vertical quartz reactor with 16 mm of inner diameter and 650 mm long. Typically, 300 mg of the catalyst are placed into the reactor and heated by an electric furnace under nitrogen flow up to the desired temperature. Then, the reactant feed, with a space velocity of 10 L(STP) g_{cat}^{-1} h^{-1}, and a total pressure of 1 atm, flows through the catalyst sample for 620 min, and the outlet flow is hourly analyzed by gas chromatography using a Varian CP4900 chromatograph. At the end the reactor is slowly cooled under nitrogen flow to room temperature. The methane conversion, carbon yield and deposition rate are determined by the difference in the reagent concentrations at the reactor inlet and outlet and a simple mass balance.

Three values of temperature, 600 °C, 650 °C and 700 °C, and three gas compositions, varying CH_4/H_2 molar flow ratio 10/0, 9/1 and 8/2, have been studied in this work. The samples have been labeled like this: X-HY, where X indicates the reaction temperature in °C, and Y indicates the hydrogen volume fraction, expressed in volume percentage, corresponding to the three tested hydrogen partial pressures: 0 atm, 0.10 atm and 0.20 atm.

2.2. Carbon nanofiber textural, structural and morphological characterization

The nature and characteristics of carbon nanofibers obtained in the experiments previously described were characterized using nitrogen physisorption, X-ray diffraction (XRD), scanning electron microscopy (SEM) and temperature programmed oxidation (TPO).

Textural properties such as specific surface area, pore volume and mesoporosity were calculated from nitrogen adsorption–desorption isotherms, measured at −196 °C using a Micromeritics ASAP 2020. Total surface area and pore volume were determined using the Brunauer–Emmet–Teller (BET) equation and the single point method, respectively. Microporosity was determined from *t-plot* method. Pore size distribution was obtained by Barret–Joyner–Halenda (BJH) method in the adsorption isotherm.

The structural properties of CNF were studied by X-ray diffraction. XRD patterns were performed using a Bruker AXS D8 Advance diffractometer, with a θ–θ configuration and using Cu Kα radiation.

The morphology of CNF was studied by SEM using a Hitachi S-3400 N. CNF diameters have been determined from SEM micrographs by direct measurement of more than 50 different fibers in three micrographs, each one in different grains in the same sample.

Finally, stability under oxidation conditions was studied by TPO. TPO experiments were carried out under a flow of air using a heating rate of 5 °C min^{-1} from room temperature up to 850 °C on a thermogravimetric analyzer Setaram.

2.3. Electrical conductivity measurements

The electrical resistance that a powdered material offers to electrical current is a combination of the individual resistances of both the grains and the contacts between them. Consequently, measuring the conductivity of a powder requires pressing on the bed of grains in order to ensure the electrical contact [30]. The device used with this purpose consists on a thick-walled PVC tube with an inner diameter of 8 mm. A scheme of the experimental set-up and the equivalent electrical circuit are shown in Fig. 1(a) and 1(b), respectively. The bottom of the cylinder is closed by a stationary brass piston and, after introducing 2 cm^3 of grinded and weighed sample, the upper side is closed by a stainless steel plunger, allowed to move down in the cylinder. Then two weighed loads are put on the upper piston and the pressure reaches values of 0.6 MPa and 1.6 MPa, which are high enough to allow good electrical contacts between grains, but too low to cause the crushing of the particles.

The height of the sample is measured by using a digital micrometer Mitutoyo with an accuracy of ±0.02 mm. Then the dc electrical

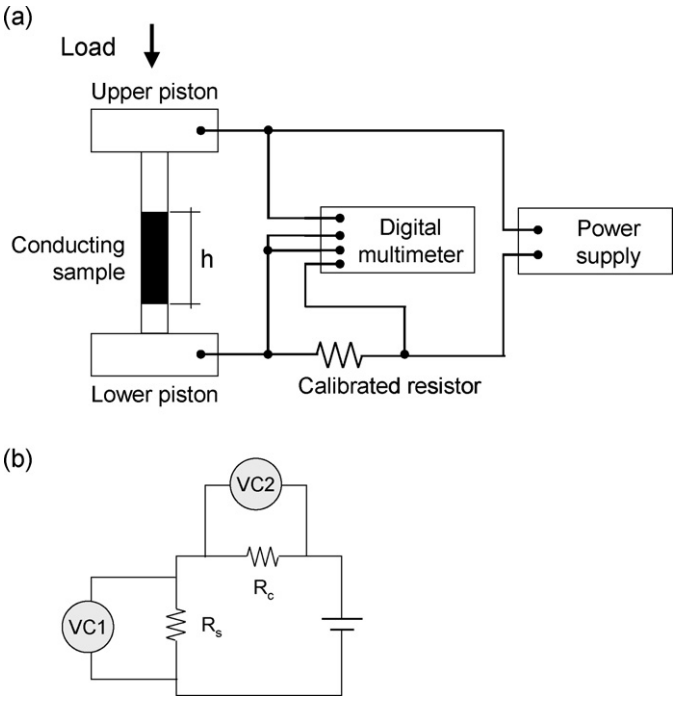

Fig. 1. (a) Scheme of the experimental devices for the measurement of electrical conductivity of carbonaceous powders and (b) equivalent electrical circuit of the device.

Table 1
Carbon nanofiber growth parameters.

Sample	Average CH_4 conversion to C (%)	Carbon yield ($gC\ g_{cat}^{-1}$)[a]	Deposition rate ($gC\ g_{cat}^{-1}\ h^{-1}$)
600-H0	18.9	9.5	0.93
600-H10	27.8	12.5	1.24
600-H20	16.6	6.7	0.65
650-H0	36.4	17.7	1.73
650-H10	36.8	15.7	1.55
650-H20	30.0	12.1	1.17
700-H0	65.8	33.2	3.29
700-H10	63.7	28.8	2.88
700-H20	56.6	22.6	2.24

[a] At the end of experiment (620 min).

resistance of the pressed powder is determined by a two-probe method. The sample and a calibrated resistor are connected acting as resistors in series, as it is schematized in Fig. 1. Known values of voltage are then applied by a power supply Array 3645A, scanning current values up to 20 mA, and voltage drop in the two resistors are measured with a 6 1/2 digits Array M3500A multimeter. Electrical conductivity is then calculated from resistance value, obtained in turn from the adjustment of voltage and current slope, and geometric parameters.

3. Results

3.1. Carbon nanofiber growth

In CNF synthesis, hydrogen might have effect on both the carbon yield, known to either accelerate or suppress carbon deposition, and also on carbon characteristics [27]. Table 1 summarizes the mean methane conversion, the final carbon yield and the mean carbon deposition rate in each synthesis condition, and Fig. 2 shows the evolution of carbon yield with time at the described experimental conditions. It is worth noting that the deposition rate is practically constant for the 10 h of experiment, indicating no significant deactivation of the catalyst. It can also be observed that, for a certain composition of the gas, increasing temperature leads to an increase in carbon yield, which can be attributed to several effects like the increase of methane conversion with temperature and a higher diffusion of carbon in the catalyst.

In the experiments performed at 600 °C (circles in the graph), a 10% of H_2 induces an increase in carbon yield from 9.5 $g_C\ g_{cat}^{-1}$ to 12.5 $g_C\ g_{cat}^{-1}$, result of a higher methane conversion. This particular behavior observed at relatively low temperatures, has been reported in methane [26] and ethylene [18,27] catalytic decomposition, in which at low concentration, hydrogen might help to remove the carbon layer which encapsulates the catalyst particle, enhancing CNF formation. Increasing the H_2 concentration up to 20% implies a reduction in the yield to 8.1 $g_C\ g_{cat}^{-1}$. At high H_2 concentrations the competition between the reactants for the metallic surface sites causes a decrease in the amount of both carbon nanofibers and encapsulating carbon species. According to Villacampa et al. [26], there is an optimal concentration of H_2 to achieve the maximum growth of CNFs, which depends on the nature of the catalyst and the operating conditions.

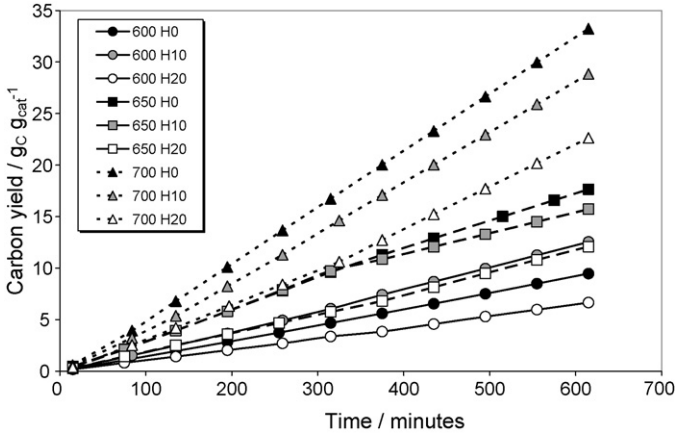

Fig. 2. CNF growth expressed in grams of carbon deposited per gram of catalyst for each tested temperature and feeding gas composition.

At a temperature of 650 °C (squares in the graph) and with a H_2 concentration of 10%, the carbon yield is practically the same as with pure methane for the first 5 h. For prolonged reaction time, the carbon yield slightly decreases, maintaining at the end a similar mean value of methane conversion (36%). Increasing H_2 concentration up to 20% leads again to a decrease in carbon yield from 17.7 $g_C\ g_{cat}^{-1}$ up to 12.1 $g_C\ g_{cat}^{-1}$, result again of a lower methane conversion. At 700 °C (triangles in the graph), increasing values of H_2 concentration imply decreasing values of carbon yield from 33.2 $g_C\ g_{cat}^{-1}$ with pure methane up to 22.6 $g_C\ g_{cat}^{-1}$ with 20% of H_2. Presumably, at 650 °C and 700 °C the hydrogen concentration that leads to a maximum carbon yield is lower than 10% under these reaction conditions. In any case, at a given temperature, low reaction rates are expected to enhance the graphitization character of deposited carbon, leading to a more ordered structure with larger crystal domain sizes [28].

3.2. Textural and morphological properties

Specific surface areas, pore volumes, average pore sizes in CNFs and CNFs average diameters estimated in SEM micrographs are summarized in Table 2. All the samples present a high mesoporosity, higher than 90% in terms of surface area and higher than 98% in terms of pore volume, which can be observed by the comparison of the columns referring mesoporous area and volume with those referring total area and volume. A high mesoporosity is desirable for their application as electrocatalyst support since platinum deposition and gas diffusion are enhanced [13]. The highest values of surface area (155.8 $m^2\ g^{-1}$) and pore volume (0.732 $cm^3\ g^{-1}$), are achieved at the lowest tested temperature, 600 °C. An increase in both the hydrogen content and/or temperature implies a decrease in both the surface area and pore volume, although the effect of temperature is more important. The effect of hydrogen on these textural properties is less influential as the temperature increases.

The morphology of these CNFs has been observed by SEM. Fig. 3 shows only two micrographs of the CNFs at different magnifications as an example, because the appearance of the CNFs in the rest images was quite similar. CNFs are present like highly entangled nanofibers a few micrometers long. The surface area in carbon nanofilaments is directly related with their diameter [31,32]. In general terms, increasing CNF diameter implies a decrease in both surface area and pore volume. CNFs diameters have been estimated by counting more than 50 nanofibers in different micrographs for each of the samples, and the average value together with the standard deviation are also shown in Table 2. Increasing reaction temperature implies increasing diameters, which explains the lower values in textural properties. The effect of hydrogen is not that clear. Firstly, at 600 °C and 650 °C there is apparently a maximum value of CNF diameter when H_2 concentration is close to 10%, but at 700 °C the diameter decreases gradually when increasing H_2 content.

3.3. Structural properties and oxidation reactivity

Carbon nanofibers graphite-like structure consists of graphitic planes arranged typically as coaxial cones, with a certain angle between graphitic layers and filament axis [16]. The average

Table 2
Textural properties of CNFs calculated from N_2 physisorption isotherms and estimated CNF mean diameter from SEM micrographs.

Sample	S_{BET} ($m^2\ g^{-1}$)	S_{meso} ($m^2\ g^{-1}$)	Pore volume ($cm^3\ g^{-1}$)	Mesopore volume ($cm^3\ g^{-1}$)	Mean pore size (nm)	CNF average diameter ± standard deviation (nm)
600-H0	155.8	140.1	0.732	0.723	6.6	53.5 ± 13.9
600-H10	129.7	117.0	0.576	0.569	6.3	60.0 ± 15.6
600-H20	134.9	122.3	0.616	0.610	6.3	56.9 ± 17.6
650-H0	123.0	112.5	0.507	0.502	6.3	63.5 ± 15.9
650-H10	121.3	108.5	0.437	0.430	6.0	72.2 ± 25.0
650-H20	126.3	112.8	0.473	0.465	6.0	61.6 ± 21.1
700-H0	107.7	99.6	0.350	0.346	6.5	80.9 ± 23.0
700-H10	102.2	94.2	0.341	0.338	6.5	73.5 ± 18.1
700-H20	93.1	86.1	0.322	0.318	6.6	69.6 ± 16.3

thickness of the stacks of parallel graphitic layers existing within the CNFs, designated L_c, can be calculated from the peak (0 0 2) in the XRD analysis obtained from a given sample. The average distance between these graphitic layers, designated d_{002}, can also be calculated. The results have been represented in Fig. 4 for all the samples. Low values of d_{002}, close to that of perfect graphite (3.354 Å), and high values of L_c are desirable in terms of structural properties. Increasing both temperature and hydrogen content leads to an improvement of structural properties since higher values of L_c are achieved. However, the interlayer distance remains approximately constant within 3.38–3.39 Å.

TPO is also a convenient technique to evaluate the extent of carbon structural order. The temperature at which the gasification reaction rate is maximum, named here as oxidation temperature,

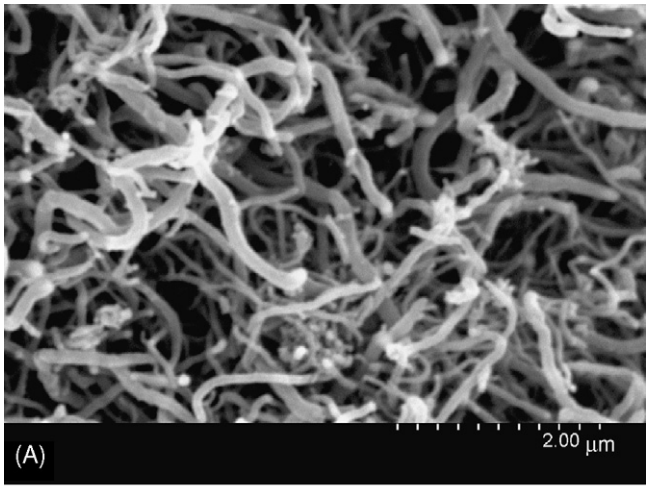

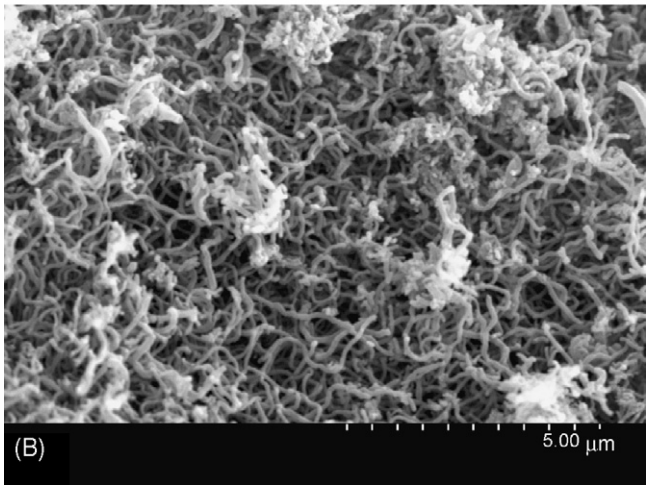

Fig. 3. SEM micrographs of carbon nanofibers at different magnifications. (a) 650-H10 and (b) 700-H10.

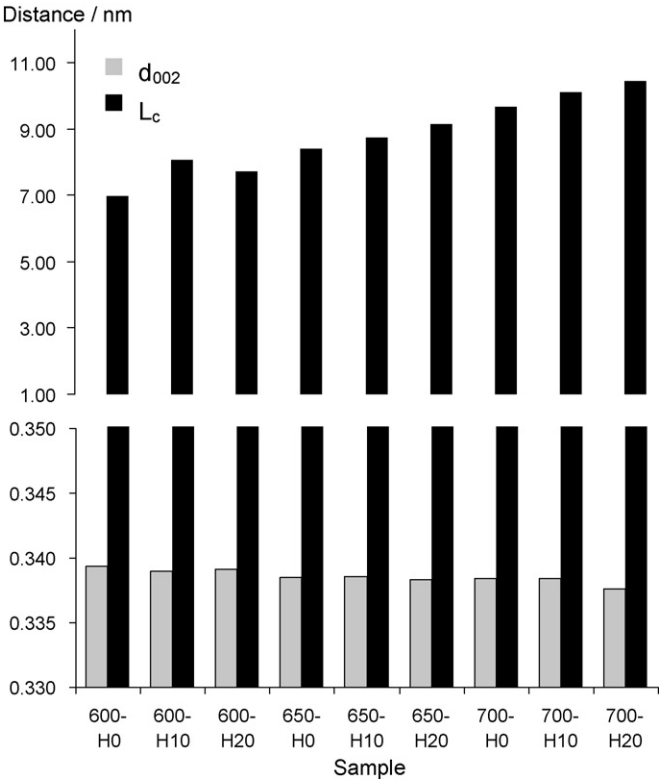

Fig. 4. Dependence of the carbon structural properties with hydrogen concentration and temperature, showing the graphite interlayer distance (d_{002}) and the crystal domain size in *c*-axis (L_c).

offers an idea of the resistance of the material towards an oxidant medium. Oxidation profiles of CNFs in TPO experiments are represented in Fig. 5 and the calculated oxidation temperatures, together with structural parameters, are presented in Table 3. The oxidation temperatures of CNFs are lower than that of graphite since they have higher surface area and more defects, which make them more reactive to oxidation.

Table 3
Structural properties from XRD patterns and oxidation temperature from TPO profiles of CNFs.

Sample	d_{002} (nm)	L_c (nm)	Oxidation temperature (°C)
600-H0	0.3394	7.0	504.4
600-H10	0.3390	8.1	522.1
600-H20	0.3391	7.7	503.5
650-H0	0.3385	8.4	513.2
650-H10	0.3386	8.7	537.2
650-H20	0.3383	9.2	534.0
700-H0	0.3384	9.7	550.9
700-H10	0.3384	10.1	541.7
700-H20	0.3376	10.5	547.5

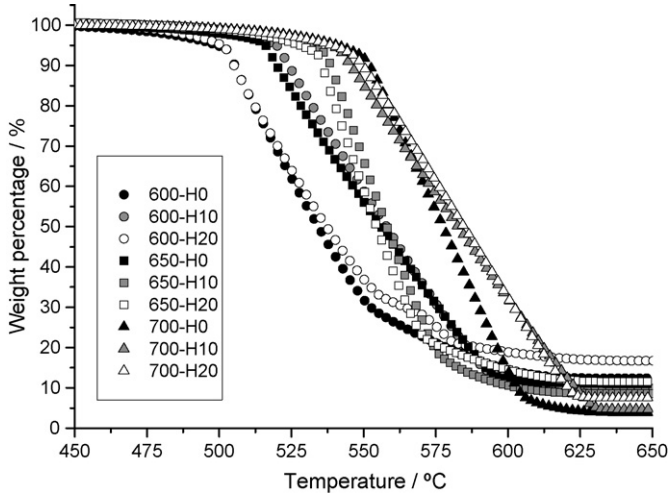

Fig. 5. Oxidation profiles of CNFs produced at different temperatures and hydrogen concentrations from TPO experiments.

The obtained results show that CNFs are oxidized in the temperature range of 500–625 °C. With pure methane in the feeding gas and synthesis temperatures of 600 °C, 650 °C and 700 °C, the oxidation temperatures are 503 °C, 513 °C and 550 °C, respectively (Table 3), corresponding with the gradual increase of crystal size observed in XRD patterns, 7.0 nm, 8.4 nm and 9.7 nm, respectively. When introducing hydrogen, CNFs obtained at reaction temperatures of 600 °C and 650 °C are oxidized at about 20 °C higher temperatures (except 600-H20), in contrast with CNFs obtained at 700 °C, in which the presence of hydrogen does not increase the oxidation temperature at the initial stage of the oxidation process. Nevertheless, at the final stage of the oxidation reaction, the temperature needed for the complete gasification of carbon is higher in the samples obtained with hydrogen (700-H10 and 700-H20) in comparison with that obtained with pure methane (700-H0). A plausible explanation is a lower content of amorphous carbon in the samples obtained with hydrogen in the reaction environment, since its reactivity towards gasification is higher than that of CNFs.

3.4. Electrical conductivity

Fig. 6 shows the electrical conductivity of the carbon nanofibers depending on the applied pressure on the powder for 0.6 MPa and 1.6 MPa. It has been reported in literature that increasing pressure implies an increase in the number of contacts between the grains and consequently electrical resistance diminishes [30,33]. What can be observed in the figure is that, for both values of pressure, the electrical conductivity of the powder increases when the reaction temperature increases for the three gaseous compositions. Analyzing the effect of hydrogen, the maximum conductivity is achieved when a 10% of H_2 is used in the CNF growth at any reaction temperature. This particular behavior suggests that electrical conductivity is not only related with structural properties because, according to XRD analyses, the conductivity of samples obtained with 20% of H_2 should be higher than those obtained with 10% H_2. Consequently, another characteristic of CNFs has to be also considered when explaining the variation of electrical conductivity. In our opinion, electrical conductivity is a complex combination of the conductivity of individual nanofilaments, the contacts between them and the contacts between the macroparticles that form the carbonaceous grains.

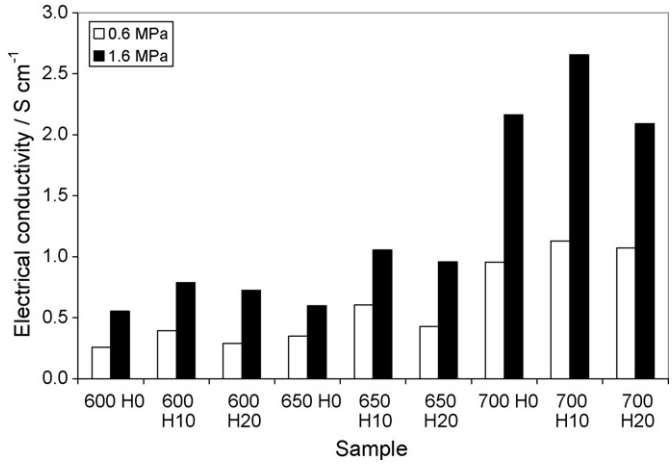

Fig. 6. Apparent electrical conductivity of the CNFs for two values of pressure: 0.6 MPa and 1.6 MPa.

Presumably hydrogen has several effects on CNFs, as it has been observed in the previous sections. Firstly, a higher ordering degree is obtained, since an increase in the crystal domain size was observed. Secondly, a lower extent of amorphous carbon is present in the carbonaceous powder when a low partial pressure of hydrogen is used. However, when increasing hydrogen concentration and temperature, lower carbon content is obtained as a result of the gasification of both amorphous and graphitic carbon. Consequently, the lower values of conductivity obtained at 20% of H_2 compared with those obtained with 10% of H_2 could be related with a decrease in the number of contacts between the nanofilaments, result of the partial gasification of CNFs.

4. Conclusions

In this study carbon nanofibers have been synthesized in a fix-bed reactor under different CH_4/H_2 compositions and at different temperatures. The powdered material has been characterized by different techniques that allow us to determine some important characteristics which are known to influence the fuel cell performance when used as electrocatalyst support.

The presence of a low partial pressure of hydrogen in the reaction gas has been shown to improve carbon structural ordering by an increase in the crystal size of about 10% with respect to the CNFs produced with pure methane. The XRD studies reveal that ordered carbon crystal sizes of 10 nm with an interlayer distance of 3.38 Å, near to graphite, can be obtained. This results in a high electrical conductivity, obtaining a maximum value when using a hydrogen concentration of 10% and high values of temperature. On the other hand, the presence of hydrogen provokes a decrease in surface area and pore volume, which are also important when considering as catalyst support, always obtaining a high mesoporosity.

Mono and bi-metallic electrocatalysts based on platinum are being synthesized using CNFs to determine the optimum formulation of the support. The subsequent studies will indicate which properties are the best in terms of high electrocatalytic activity, durability and fuel performance.

Acknowledgements

The authors gratefully acknowledge financial support given by the Aragon Government under the project PM042/2007. D. Sebastián also acknowledges CSIC for his I3P predoctoral grant.

References

[1] H.A. Gasteiger, S.S. Kocha, B. Sompalli, F.T. Wagner, Applied Catalysis B: Environmental 56 (2005) 9–35.
[2] E. Passalacqua, F. Lufrano, G. Squadrito, A. Patti, L. Giorgi, Electrochimica Acta 43 (1998) 2665–3673.

[3] J. Ding, K.-Y. Chang, J. Ren, F.-S. Xiao, Electrochimica Acta 50 (2005) 3131–3141.
[4] S.H. Joo, C. Park, D.J. You, S.-A. Lee, H.-I. Lee, J.M. Kim, H. Chang, D. Seung, Electrochimica Acta 52 (2006) 1618–1626.
[5] L. Calvillo, M.J. Lázaro, E. García-Bordejé, R. Moliner, P.L. Cabot, I. Esparbé, E. Pastor, J.J. Quintana, Journal of Power Sources 169 (2007) 59–64.
[6] J. Marie, S. Berthon-Fabry, P. Achard, M. Chatenet, A. Pradourat, E. Chainet, Journal of Non-Crystalline Solids 350 (2004) 88–96.
[7] P.V. Samant, J.B. Fernandes, C.M. Rangel, J.L. Figueiredo, Catalysis Today 102 (2005) 173–176.
[8] J.L. Figueiredo, M.F.R. Pereira, P. Serp, P. Kalck, P.V. Samant, J.B. Fernández, Carbon 44 (2006) 2516–2522.
[9] C. Arbizzani, S. Beninati, E. Manferrari, F. Soavi, M. Mastragostino, Journal of Power Sources 172 (2007) 578–586.
[10] C.A. Bessel, K. Laubernds, N.M. Rodriguez, R.T.K. Baker, The Journal of Physical Chemistry 105 (6) (2001) 1115.
[11] Z.R. Ismagilov, M.A. Kerzhentsev, N.V. Shikina, A.S. Lisitsyn, L.B. Okhlopkova, Ch.N. Barnakov, M. Sakashita, T. Ijima, K. Takodoro, Catalysis Today 102–103 (2005) 58–66.
[12] A. Gangeri, G. Centi, A. La Malfa, S. Perathoner, R. Vieira, C. Pham-Huu, M.J. Ledoux, Catalysis Today 102 (2005) 50–57.
[13] K. Lee, J. Zhang, H. Wang, D.P. Wilkinson, Journal of Applied Electrochemistry 36 (2006) 507–522.
[14] C. Wang, M. Waje, X. Wang, J.M. Tang, R.C. Haddon, Y. Yan, Nano Letters 4 (2004) 345–348.
[15] N.M. Rodriguez, Journal of Materials Research 8 (1993) 3233–3250.
[16] T.V. Reshetenko, L.B. Avdeeva, Z.R. Ismagilov, V.V. Pushkarev, S.V. Cherepanova, A.L. Chuvilin, V.A. Likholobov, Carbon 41 (2003) 1605–1615.
[17] F. Zaragoza-Martín, D. Sopeña-Escario, E. Morallón, C. Salinas-Martínez de Lecea, Journal of Power Sources 171 (2007) 302–309.
[18] P. Serp, M. Corrias, P. Kalck, Applied Catalysis A: General 253 (2003) 337–358.
[19] A. Romero, A. Garrido, A. Nieto-Márquez, A.R. de la Osa, A. de Lucas, J.L. Valverde, Applied Catalysis A: General 319 (2007) 246–258.
[20] E. Hammel, X. Tang, M. Trampert, T. Schmitt, K. Mauthner, A. Eder, P. Pötschke, Carbon 42 (2004) 1153–1158.
[21] K.P. de Jong, J.W. Geus, Catalysis Reviews Science and Engineering 42 (2000) 481–510.
[22] T.V. Reshetenko, L.B. Avdeeva, Z.R. Ismagilov, A.L. Chuvilin, V. Ushakov, Applied Catalysis A: General 247 (2003) 51–63.
[23] V.B. Fenelonov, A.Y. Derevyankin, L.G. Okkel, L.B. Avdeeva, V.I. Zaikovskii, E.M. Moroz, A.N. Salanov, N.A. Rudina, V.A. Likholobov, S.K. Shaikhutdinov, Carbon 35 (1997) 1129–1140.
[24] J. Chen, Y. Li, Y. Ma, Y. Qin, L. Chang, Carbon 39 (2001) 1467–1475.
[25] G.G. Kuvshinov, Y.I. Mogilnykh, D.G. Kuvshinov, V.I. Zaikovskii, L.B. Avdeeva, Carbon 36 (1998) 87–97.
[26] J.I. Villacampa, C. Royo, E. Romeo, J.A. Montoya, P. Del Angel, A. Monzón, Applied Catalysis A: General 252 (2003) 363–383.
[27] Z. Yu, D. Chen, B. Tøtdal, A. Holmen, Materials Chemistry and Physics 92 (2005) 71–81.
[28] J.L. Pinilla, I. Suelves, M.J. Lázaro, R. Moliner, J.M. Palacios, International Journal of Hydrogen Energy 33 (2008) 2515–2524.
[29] I. Suelves, M.J. Lázaro, R. Moliner, Y. Echegoyen, J.M. Palacios, Catalysis Today 116 (2006) 271.
[30] A. Celzard, J.F. Marêché, F. Payot, G. Furdin, Carbon 40 (2002) 2801–2815.
[31] M.L. Toebes, Y.H. Zhang, J. Hajek, T.A. Nijhuis, J.H. Bitter, A.J. van Dillen, D.Y. Murzin, D.C. Koningsberger, K.P. de Jong, Journal of Catalysis 226 (2004) 215–225.
[32] M.K. Van der Lee, A.J. van Dillen, J.W. Geus, K.P. de Jong, J.H. Bitter, Carbon 44 (2006) 629–637.
[33] D. Pantea, H. Darmstadt, S. Kaliaguine, L. Sümmchen, C. Roy, Carbon 39 (2001) 1147–1158.